Summer Internship Project
Report

Calibration of EJ-301 Organic Liquid Scintillating Detector and Discriminating Neutrons and Gamma from Am-Be

Submitted by

Dhiman Baruah
Firts year

Under the guidance of

Dr. Bedangadas Mohanty and Sudipta Das

Center for Medical and Radiation Physics (CMRP)
National Institute of Science Education and Research

Summer Internship 2025

Calibration EJ-301 Organic Liquid Scintillating Detector and Discriminating Gamma and Neutrons interaction events in Am-Be

Abstract

We studied the response of an EJ-301 organic liquid scintillation detector to gamma and neutrons with the help of an Am-Be source. Am-Be is a commonly used fast neutron ($\mathcal{O}$ (MeV)) source that exhibits a continuous neutron spectrum. In addition, it also emits gamma. The EJ-301 organic scintillating detector shows different detector responses to neutrons and gamma rays. We calibrated the detector using standard gamma sources, and discriminated the gamma and neutron events from the Am-Be source using the pulse-shape discrimination (PSD) technique.

1 Introduction

Organic liquid scintillating detectors have the characteristic of converting the kinetic energy of interacting charged particles into detectable light (photons). In an organic liquid scintillating detector like that of EJ-301, there is a high concentration of hydrogen atoms. When fast neutrons from the Am-Be source enter the medium of the detector, the recoil of the protons as well as nuclei takes place. The energy of the recoiled proton is absorbed by electrons in various energy levels of the π electrons present in the aromatic rings of the organic liquid scintillating. In case of gamma interaction, mainly Compton scattering takes place, which has a higher contribution of recoiled electrons.

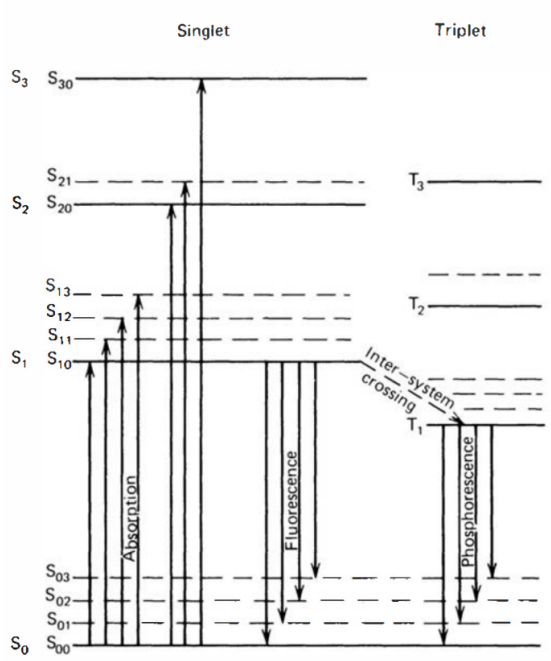

Figure 1: Energy levels of an organic molecule with π-electron structure [1].

The scintillation from the detector has two components: The Fast and Slow Components. The fast component is the prompt fluorescence that takes place from the first singlet state (S_1) to the ground state (S_0). The slow component is the delayed fluorescence that takes place due to forbidden transitions like: $T_1 \rightarrow S_0$, $T_0 + T_0 \rightarrow S_1 + S_0 + \text{Phonon}$; where T_1, T_0 is the first and ground triplet states, respectively. The lifetime for the first triplet state T_1 is characteristically much longer than that of the singlet state S_1. The lifetime of T_1 may be as much as 10^{-3}s, whereas that of fluorescence is roughly 10^{-8}s. It is because when the electron de-excites from T_1 to S_0, the spin of the electron is altered due to Pauli's exclusion principle. Moreover, through a transition called inter-system crossing, some excited singlet states may be converted into triplet states. The radiation emitted in a de-excitation from T_1 to S_0 is therefore a delayed light emission characterised as phosphorescence, which constitutes the slow component. The Jablonski diagram of the π-electronic energy levels of the molecules present in the organic scintillating detector is shown in Figure-1.

With respect to the explanation in the first paragraph of Section-1, due to the higher mass of the recoiled protons and nuclei, they have a higher rate of loss of energy ($\frac{dE}{dx}$) as compared to the recoiled electron. A high ($\frac{dE}{dx}$) produces a high density of excited molecules, which results in higher intermolecular interactions. These reactions hinder the normal singlet internal degradation process, which leads to the radiative S_1 state by draining their energy through other channels. As a result, the proportion of the fast component emitted relative to the slow component is thus reduced, especially in the case of recoiled protons and

nuclei, which is mainly created by neutron interaction. While the gamma interaction mainly creates recoiled electrons, which have a lesser $\frac{dE}{dx}$ than protons and nuclei because of their smaller mass. Hence, the light output due to the gamma has a higher contribution of the faster component compared to the neutron interaction.

The light emitted from the scintillating detector now enters the Photo-Multiplier Tube (PMT). PMT is basically composed of a photocathode followed by an electron collection system, an electron multiplier section and an anode. The incident photons from the scintillating detector on the photocathode cause electron emission due to the photoelectric effect. The photo-electron stream is then directed and focused towards the first section of the photomultiplier, which happens to be a series of dynodes. It is done by the application of electric and magnetic fields. The function of the dynodes is to amplify the weak primary photocurrent. Thus, the amplified electron stream which reaches the anode produces a pulse. Thus, the nature of the pulse is proportional to the light output, i.e. energy deposition from the radioactive source, which is digitally extracted and processed to get the required information.

2 Experimental Setup

The liquid scintillation detector used here is EJ-301, manufactured by Eljen Technology. It is coupled to a Photo Multiplier Tube (PMT) of model number R7724, devised by Hamamatsu. We found that 900V gave good discrimination for Neutron and Gamma. Hence we took the voltage to be 900V. The output from the anode of PMT is fed to a CAEN V1730 digitizer (14 bit) which performs Digital Pulse Processing (DPP) for Pulse-Shape Discrimination (PSD) by the charge integration method.

3 Calibration of the detector

Calibration is the process of comparing an instrument's reading to known standard data and establishing a relationship between between them. A current pulse is generated by the PMT as a result of the energy transfer. Higher the area under the pulse higher is the energy deposition on the medium of the detector.The area under the pulse is then computed (total charge), which has to be proportional to the energy deposition. The total charge integration is digitised by the Analog-to-Digital Converter (ADC). Thus Higher energy depositon corresponds to a high channel number. So, the actual Energy deposition in relation to the channel number is given by the equation:

$$Energy = m \times (ADC\ Channel) + c$$

where m and c are callibration parameters.

In our case, the calibration of the EJ-301 scintillating detector is done by Na-22 and Cs-137 gamma sources. The energy of the Gamma photons of Na-22 and Cs-137 is given in the table-1. The first and second edges of Na-22 are referred to as the edge between 250 and 500 ADC channels and 1250 and 1000 ADC, respectively, in the ADC spectrum of Na-22 in Table-1 The mentioned Energies in Table-1 are taken from reference [2] and [3]. The ADC spectrum of Na-22 and Cs-137 obtained from the detector is shown in Figure 2. It must be noted that, in both plots, the spike before 250 ADC is due to noise and the digitiser's threshold effect[4]. It can be seen that there exist two edges: one between 250 and 500 ADC, while the other edge is between 1250 and 1500 ADC. Moreover, another edge can also be seen between 500 and 700 ADC of the Na spectrum in fig-2, which closely resembles the Compton peak of Cs-137. The detailed explanation of this observation is explained in Section-4.1.

Sources	**Energy of Gamma Photons in MeV**
Na 22 (first edge)	0.5110
Na 22 (second edge)	1.2745
Cs 137	0.6617

Table 1: The respective literature energies of Gamma photons of Na-22 and Cs-137.

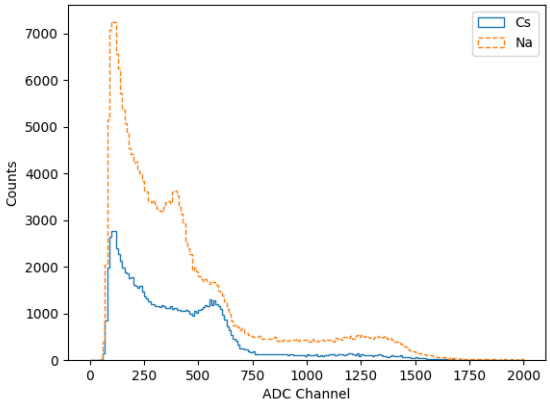

Figure 2: ADC spectrum of Na-22

3.1 Method used for locating the edges

Each midpoint of the histogram bins is fitted with an error function. The fitted curve for the edge between the 1250 and 1500 ADC channels is shown in Figure 4. As used in reference-[5], the edge happens to be the minimum value of the derivative of the fitted error function, which is found to be approximately at 1474 ADC channels for Na-22 in Figure-4. The same procedure is used for obtaining the edge between 250 and 500 ADC channels of Na-22. The fitted curve for the edge is shown in the figure 3, and the edge is found to be at approximately 4478 ADC channel.

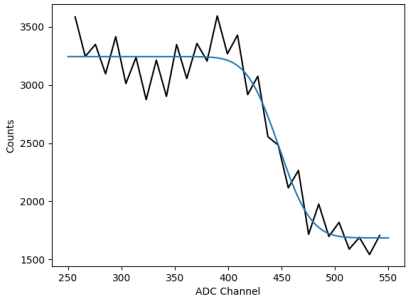

Figure 3: Fitted curve for the first edge of Na-22

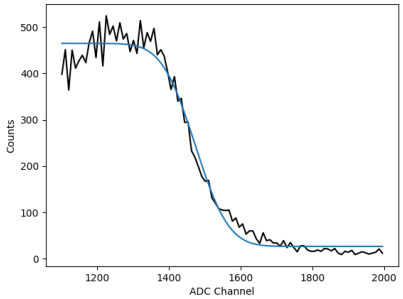

Figure 4: Fitted curve for the second edge of Na-22

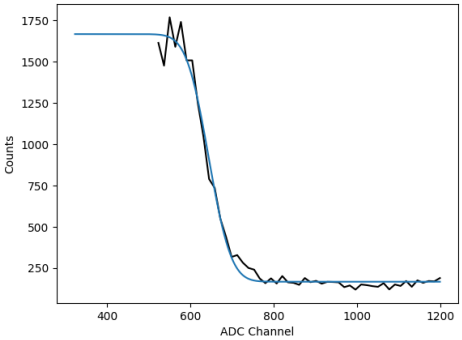

Figure 5: Fitted curve for Cesium-137

The fitted curve for the edge that appears between 500 and 750 ADC channels of Cs-137 (in Figure-2) is shown in Figure-5. On applying the same procedure mentioned above, the edge is found to be at approximately at 644 ADC.

3.2 Obtaining the relation between ADC channel and Energy deposition

In order to calculate the energy of the Compton edge (energy deposited at 180^o scattering angle, $E_{deposited}$) for each of the Gamma source, the following equation is used:

$$E_{deposited} = \frac{2E^2}{mc^2 + 2E}$$

Here, E is the energy of the Gamma photons and m is the mass of the electron. The respective values of E for each element is given in table-1. The calculation of the Compton edge energy for the Cs-137 is shown below:

$$E_{deposited} = \frac{2 \times 0.6617^2}{0.511 + 2 \cdot (0.6617)}$$
$$E_{deposited} = 0.4777 MeV$$

Similar procedure is used for calculating the Compton edges of Na-22. The respective Compton edge Energies of Cs and Na and there corresponding ADC channel are given in the Table-2.

Sources	ADC Channel	Compton Edge Energy in MeV
Cs 137	644.174137682	0.4777
Na 22 (first edge)	447.56066337	0.3467
Na 22 (second edge)	1473.49098918	1.0617

Table 2: The respective literature energies at which the corresponding edges were observed.

From the preceding discussion, it is clear that Energy and ADC Channel number should obey a linear relationship. Hence, the plot of Energy versus ADC Channel is fitted for the equation: $y = mx + c$ as shown in the Figure 6. It has been observed that the error bars for the plot along the ADC channel axis are way too small (around 2 units in all three cases) to be visible as compared to the scale. It is because the total number of bins is taken to be 200 in the histograms of Na-22 and Cs-137. As a result, the standard deviation obtained in each bin is quite low. The equation of the fitted curve is: $y = (0.007032 \pm 0.000001)x + (0.025 \pm 0.001)$

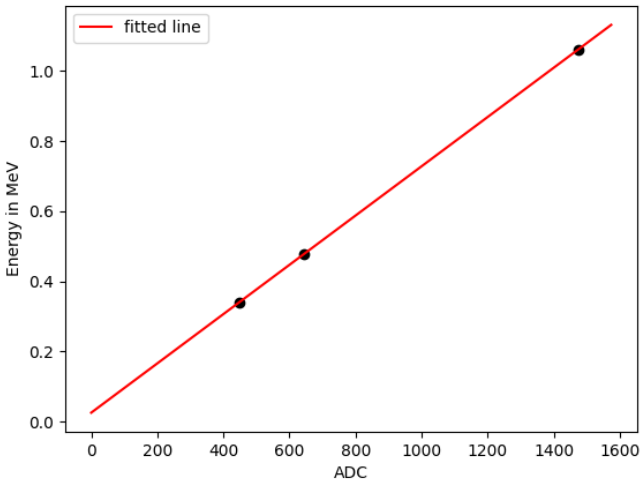

Figure 6: The fitted plot of Energy versus ADC Channel

4 Reviewing the Energy spectra after the calibration

The energy spectra of Na-22 and Cs-137 obtained after the calibration are shown in Figure-7 and 8 respectively.

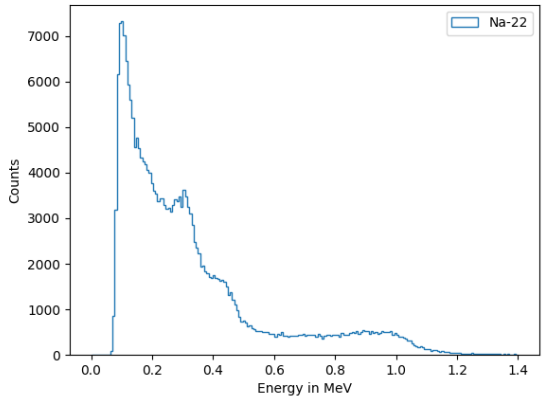

Figure 7: Energy spectrum of Na-22

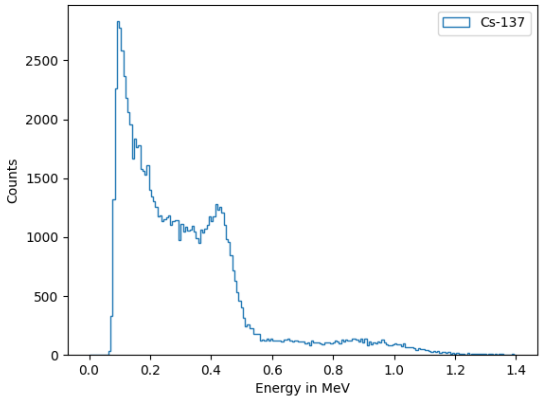

Figure 8: Energy spectrum of Cs-137

4.1 Explanation for the unusual peak observed in the Na-22 spectrum

As discussed in section-3, the edge between 500 and 750 ADC of Na-22 as seen in the figure-2, closely matches with Compton edge of Cs-137. The fitted curve of the region is shown in Figure-9. From the obtained error function, the edge is found to be approximately at 636 ADC, which corresponds to approximately 0.473 MeV. It must be noted that the energy at which the edge is observed closely resembles the energy at which the Compton edge takes place in Cs-137 (Table-2). So, this confirms that contamination of Gamma photons from the Cs-137 took place, which might be kept near the Na-22 while taking the data for Na-22.

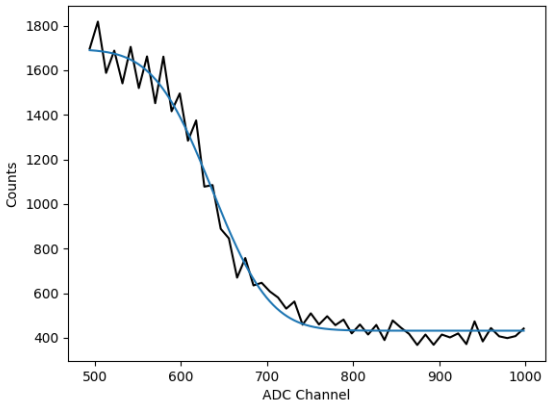

Figure 9: The fitted plot of the unusual edge in the ADC spectrum of Na-22

5 Obtaining the spectrum of Am-Be

The Am-Be source is composed of Am-241 and Be-9. It emits neutrons by the following chain reaction: $^{241}\mathrm{Am} \longrightarrow {}^{237}\mathrm{Np} + \alpha$, $^{9}\mathrm{Be} + \alpha \longrightarrow {}^{12}\mathrm{C}^{*} + n$. The final carbon atom (C^{*}) is generally an excited nucleus, decays into its ground state, emitting Gamma photons[6]. Hence, Am-Be acts as both a Gamma and Neutron Source. The Energy spectrum of Am-Be is shown in Figure-10

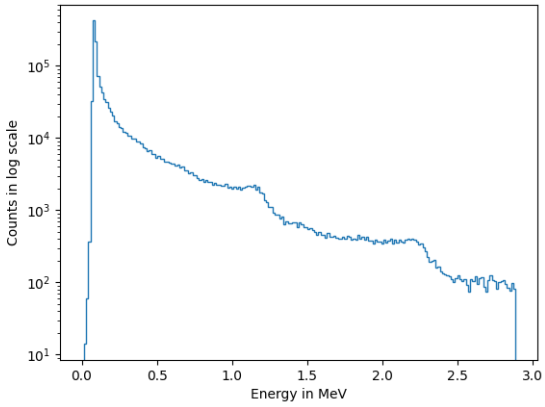

Figure 10: The Energy spectrum of Am-Be

6 Pulse-Shape Discrimination (PSD) for Am-Be

The PSD parameter is defined as:

$$PSD = 1 - \frac{Q_s}{Q_l}$$

where Q_s is the integrated charge in the short gate and Q_l is the integrated charge in the long gate. We have chosen the gate values to be 40 ns and 280 ns for the short and long gates, respectively. As discussed in section-1, the current pulse output from the PMT is directly proportional to the scintillation from the detector due to which, the recoiled protons and nuclei due to neutron interaction result in the light output that has a higher "slow component" than that of electron recoils by Gamma interaction. As a result, the integrated charge output in the long gate has a higher value as compared to that of the Gamma interaction. While, the integrated charge output in the short gate has a lower value in the Neutron interaction as compared to the Gamma interaction. Let $(Q_s)_n$, $(Q_l)_n$ be the integrated charge in neutron interaction in the short and long gate respectively, and $(Q_s)_\gamma$, $(Q_l)_\gamma$ be the integrated charge in Gamma interaction in the short and long gate respectively. Then,

$$(Q_s)_n < (Q_s)_\gamma \tag{1}$$

$$(Q_l)_n \approx (Q_l)_\gamma$$

$$\Rightarrow \quad \frac{1}{(Q_l)_n} \approx \frac{1}{(Q_l)_\gamma} \tag{2}$$

From (1) and (2),

$$\Rightarrow \quad \frac{(Q_s)_n}{(Q_l)_n} < \frac{(Q_s)_\gamma}{(Q_l)_\gamma}$$

$$\Rightarrow \quad \frac{(Q_s)_n}{(Q_l)_n} < \frac{(Q_s)_\gamma}{(Q_l)_\gamma}$$

$$\Rightarrow \quad 1 - \frac{(Q_s)_n}{(Q_l)_n} > 1 - \frac{(Q_s)_\gamma}{(Q_l)_\gamma}$$

$$\Rightarrow \quad (PSD)_{Neutron} > (PSD)_\gamma$$

Thus, ideally, the PSD parameter obtained from Neutron interactions is always greater than the PSD parameter due to the Gamma interaction.

The PSD versus Energy of Am-Be is shown in figure-11. It can be seen that a clear separation of the bands due to Neutron interaction and Gamma interaction takes place. From the above derivation, it is clear that the upper band corresponds to the Neutron interaction while the lower band corresponds to the Gamma interaction. It is evident from the plot that the counts of the Gamma interaction are higher than those of the neutron interaction. It suggests that the source (Am-Be) has higher Gamma emission as compared to Neutron emission.

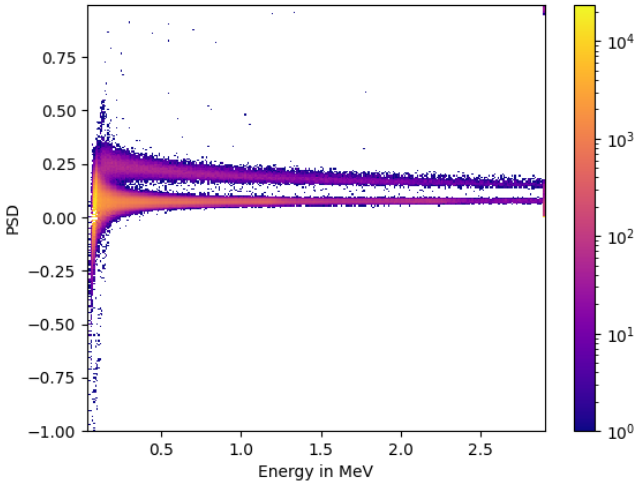

Figure 11: 2D Histogram plot for Energy versus PSD of Am-Be

6.1 Obtaining the Neutron and Gamma Spectrum of Am-Be

In order to obtain the Neutron and Gamma spectra separately, the 2-D histogram of Am-Be (Figure-11) obtained above is sliced at 0.136 PSD and 0.39 MeV by ensuring that the upper band corresponds (for the Neutron interaction) to PSD $>$ 0.139 and Energy $>$ 0.39 MeV. In the same way, the lower band corresponds to (for the Gamma interaction) PSD $<$ 0.139 and Energy $>$ 0.39 MeV, which is evident from the 2D plot. The sliced plot of the above 2-D histogram of Am-Be is shown in figure-12 and 13. The slicing in such that the both the bands had the least amount of overlap.

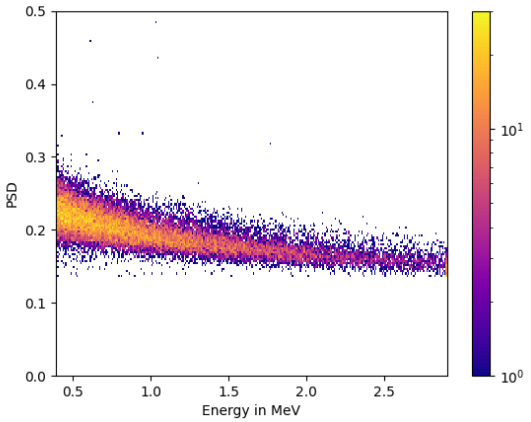

Figure 12: 2D Histogram plot for Energy versus PSD of Am-Be for the upper band(in fig-11)which corresponds to the Neutron interaction

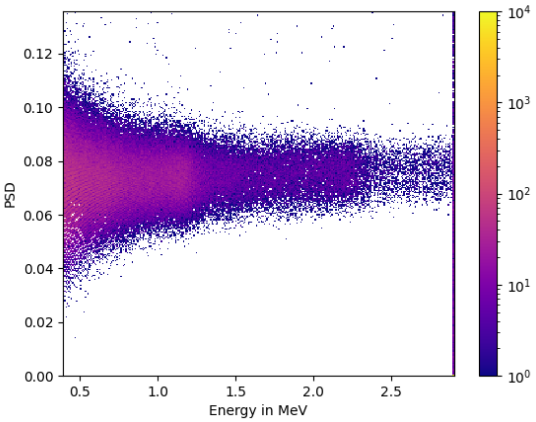

Figure 13: 2D Histogram plot for Energy versus PSD of Am-Be for the lower band (fig-11) which corresponds to the Gamma interaction

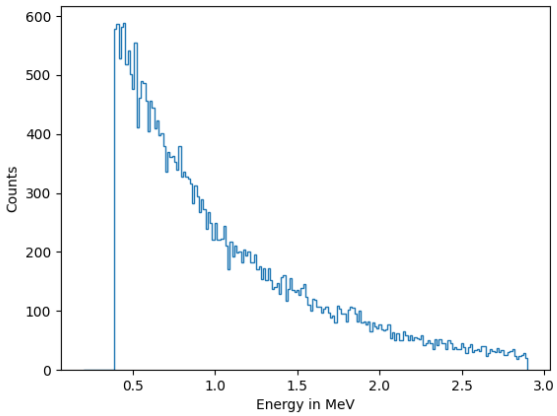

Figure 14: Energy spectrum of Neutron interaction events of Am-Be

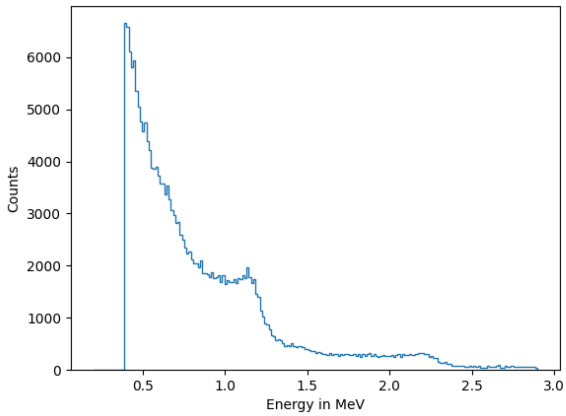

Figure 15: Energy spectrum of Gamma interaction events of Am-Be

From the plots shown in Figure-12 and Figure-13, the Energy spectrum of Neutron and Gamma events is separately obtained, which is shown in the figure-14 and figure-15 respectively. It can be seen that there exists an edge in Figure-15 between 1.0 and 1.5 MeV, which corresponds to the Compton edge of the Gamma spectrum of Am-Be. The fitted curve of the edge is shown in Fig. **??**. The edge happens to be at 1.243 MeV, which corresponds to the energy deposition by 1.458 MeV gamma photons. We know that potassium-40 (K-40) has gamma photons of energy 1.460 MeV, which happens to be the highest background Gamma source. Hence, the edge corresponds to the Compton edge observed due to gamma photons from K-40.

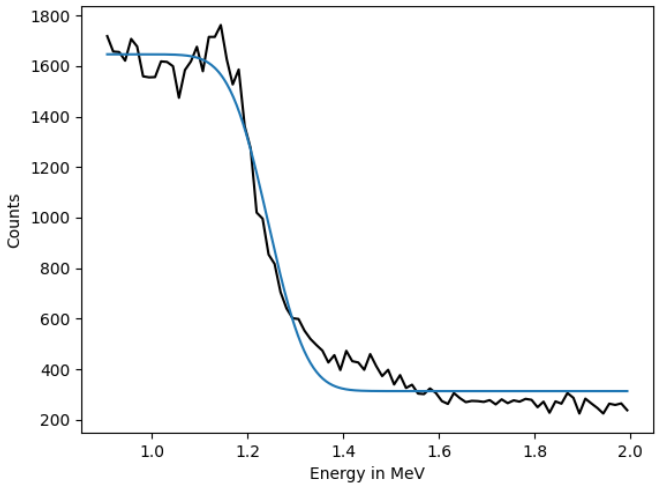

Figure 16: Fitted curve for the edge between 1.0 and 1.5 Mev in fig-15

7 Conclusion

In this project, the EJ-301 organic liquid scintillating detector is successfully calibrated using known gamma sources, i.e. Na-22 and Cs-137. A linear relationship between ADC channel number and Energy deposition is established. The calibration allowed the display of the PSD of Am-Be with its corresponding energies. Using the pulse shape discrimination technique, we distinctly separated neutron events from gamma interactions, which demonstrates the detector's effectiveness in dual-radiation environments. This study confirmed the expected physical behaviour of scintillation processes in EJ-301, as well as validated the use of charge-integration PSD for real-time radiation discrimination, which plays an important role in identifying the different types of radiation interaction from a mixed radiation source.

References

[1] William R. Leo. *Techniques for Nuclear and Particle Physics Experiments: A How-to Approach.* Springer-Verlag Berlin Heidelberg, second revised edition edition, 1994.

[2] Sodium-22 radiological safety guidance. Technical Report Revision Date: 09/20/18, Radiation Safety Office, sep 2018. Accessed from Sodium-22 data sheet PDF.

[3] James E. Parks and Christine P. Cheney. Compton scattering of cs-137 gamma rays. In *2015 Conference on Laboratory Instruction Beyond the First Year (BFY II)*, pages 76–79. American Association of Physics Teachers, 2015. Edited by Eblen-Zayas, Behringer, and Kozminski.

[4] S. Das, V.K.S. Kashyap, and B. Mohanty. Energy calibration of ej-301 scintillation detector using unfolding methods for fast neutron measurement. *Nuclear Instruments and Methods in Physics Research Section A: Accelerators, Spectrometers, Detectors and Associated Equipment*, 1042:167405, 2022.

[5] M. J. Safari, F. Abbasi Davani, and H. Afarideh. Differentiation method for localization of compton edge in organic scintillation detectors. *Radiation Measurements*, 94:52–59, 2016.

[6] Hiroshi Ito, Kohei Wada, Takatomi Yano, Yota Hino, Yuga Ommura, Masayuki Harada, Akihiro Minamino, and Masaki Ishitsuka. Analyzing the neutron and -ray emission properties of an americium–beryllium tagged neutron source. *Nuclear Instruments and Methods in Physics Research Section A: Accelerators, Spectrometers, Detectors and Associated Equipment*, 1057:168701, 2023.